High energy laser heating and ignition study

K. C. Lee[a], K. H. Kim[a] and J. J. Yoh[a]
[a]Department of Mechanical and Aerospace Engineering,
Seoul National University, Seoul, 151-742, Korea
jjyoh@snu.ac.kr

Keywords: Energetic materials, Laser heating, Ignition, Explosion.

Abstract

We present a model for simulating high energy laser heating and ignition of confined energetic materials. The model considers effect of ablation of steel plate with long laser pulses and continuous lasers of several kilowatts and the thermal response of well-characterized high explosives for ignition. Since there is enough time for the thermal wave to propagate into the target and to create a region of hot spot in the high explosives, electron thermal diffusion of ultra-short (femto- and pico-second) lasing is ignored; instead, heat diffusion of absorbed laser energy in the solid target is modeled with thermal decomposition kinetic models of high explosives are used. Numerically simulated pulsed-laser heating of solid target and thermal explosion of cyclotrimethylenetrinitramine (RDX), triaminotrinitrobenzene (TATB), and octahydrotetranitrotetrazine (HMX) are compared to experimental results. The experimental and numerical results are in good agreement.

Introduction

A pulsed laser or high intensity continuous laser irradiation on the surface of solid material causes rapid temperature increase beyond the evaporation temperature inducing explosive phase changes on the surface. During the process, the evaporated materials quickly expand while generating high pressure shock waves and leaving behind a crater of its beam diameter size. The energy transferred from the high energy irradiation to the material particles yield increased momentum and induce material particles to move with high velocities away from the surface, causing ablation of the material. The process of ablation and thermal effects by pulsed lasers has been extensively studied by numerous researchers [1-3].

The laser flux of present study ranges in several thousand joules per cm^2, and the length of the irradiation is short enough to cause no excessive removal of beamed surface of the target. During the course of laser heating of a steel plate, the thermal wave initiated from the surface reaches the rear end of a 1.5 mm thick plate and eventually causes the inside energetic material to ignite. Two pathways for the laser ignition are possible; first, the heat is conducted through the metallic shield until heating the confined energetic material until ignition, and second, the purely hydrodynamic shock wave through the laser drilled hole carries enough energy to mechanically ignite the energetic material behind the shield. However, the latter possibility of mechanical ignition via laser driven shock wave is discussed in the forthcoming paper, instead, entirely thermal ignition is assumed since the ablation depth relative to the metal thickness is small in the present analysis.

Unlike in the ultra short pulse (femto- or pico-second) irradiation that considers two separate temperatures for electron and lattice, the present long pulse (> nanosecond) energy transport is best described by a single temperature diffusion model [4]. For the 10 kW pulsed solid state heat capacity laser (SSHCL) and for two continuous-wave CO_2 lasers, one temperature model with multi-step thermal decomposition reaction model for high explosives are adapted [5]. We focus on the thermal response of materials without the mechanical transport, providing a simple and accurate comparison of the modeled results and the experimental data of [5, 6]. Our model includes the convective and conductive transport on the metallic target with the irradiative energy transfer from the high energy lasers. We develop three- and four- step deflagration kinetics of high explosives subject to direct laser irradiation. This combination of high energy laser heating and confined energetic material ignition modeling provides a first time attempt at establishing the performance index of high energy laser weapon system.

Problem description

We consider a heat flow from a millisecond high energy laser (HEL) source to a metal and to a confined energetic material inside a metal container. The thickness of steel target is 1.5 mm with 50.8 mm width and 127 mm height. The high energy source is provided by a 10 kW SSHCL operated at 20 Hz frequency, with pulse energy of 500 J and duration of 0.5 ms [7]. Laser beam is focused to an area of 5 cm^2, resulting in 100 J/cm^2 of fluence. The ignition of energetic materials is considered through affixing a layer of high explosive (RDX) to a metal target. Figure 1 shows two cases of laser-target interaction experiment.

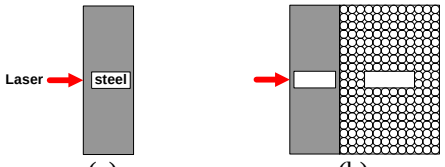

FIGURE 1. Two cases of pulse energy transfer to a steel (a) without RDX and (b) with RDX in contact.

The solution procedure is divided into two steps: first, the energy transfer in steel is considered first. The irradiation from the HEL quickly heats the front side of a steel plate. Heat flux from the front is conducted through the back side via thermal diffusion. Second, the back side of steel is in contact with an energetic material, which is then progressively heated by the multiple laser pulses until explosion occurs.

In addition to confined explosive ignition analysis, we also conduct calculations of unconfined explosive ignitions using HEL. Instead of a pulsed-laser, two continuous-type CO2 lasers (Edinburgh Instruments Ltd. PL-6, 180 W, and PRC Corp. SL 1000, 1000 W) are used to ignite the high explosives [6]. The intensity ranges from 10 to 1000 W/cm^2, and the choice of explosives are the TATB and HMX [6, 8]. This continuous-type laser ignition of the high explosive pellets of 1cm diameter and 6.4 mm thickness is analogous to the classical one-dimensional-time-to-explosion (ODTX) test for characterizing energetic materials.

Mathematical formulations

The heat transfer in steel plate is considered through the one dimensional diffusion equation.

$$\rho_s C_{p_s} \frac{\partial T}{\partial t} = k_s \frac{\partial^2 T}{\partial x^2} \tag{1}$$

where ρ_s, C_{Ps} and k_s are density, specific heat, and thermal conductivity of steel, respectively. Specific heat and thermal conductivity coefficients are thermally dependant as shown in figure 2.

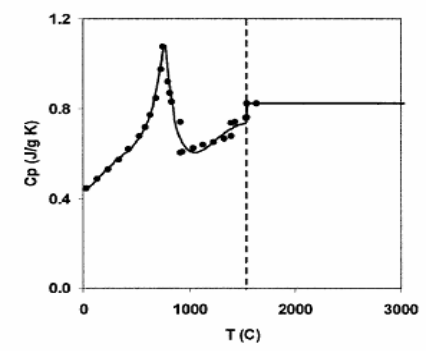

(a)

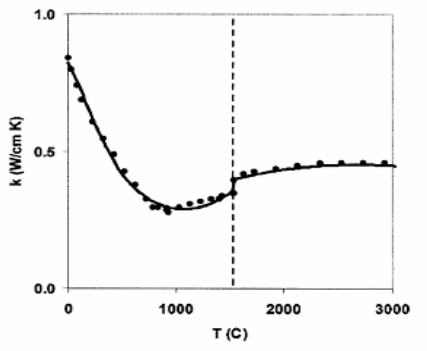

(b)

Figure 2. Thermal dependence of coefficients of steel: (a) Specific heat [9], (b) Thermal conductivity [10].

As for the case of confined explosion by laser irradiation, the chemical heat release term is added to the equation as

$$\rho_e C_{p_e} \frac{\partial T}{\partial t} = k_e \frac{\partial^2 T}{\partial x^2} + \sum_{i=1}^{N} r_i q_i \tag{2}$$

Here ρ_e, C_{Pe} and k_e are density, specific heat and thermal conductivity of energetic material, respectively. r_i is reaction rate, and q_i is the heat of reaction. N is the total number of chemical reaction steps.

The process of laser induced heating leads to a class of fast deflagration phenomena where the thermal decomposition of high explosive occurs, followed by a rapid gaseous exothermic reaction. A three-step chemical decomposition mechanism for RDX and TATB are considered while a four-step mechanism is proposed for HMX as suggested in [11]. The 4 step chemical reaction, for instance, is written as

$$A \rightarrow B, \quad r_1 = Z_1 \exp(-E_1 / RT)\rho_A \tag{3}$$

$$B \rightarrow C, \quad r_2 = Z_2 \exp(-E_2 / RT)\rho_B \tag{4}$$

$$C \rightarrow D, \quad r_3 = Z_3 \exp(-E_3 / RT)\rho_C \tag{5}$$

$$D \rightarrow E, \quad r_4 = Z_4 \exp(-E_4 / RT)\rho_D^2 \tag{6}$$

where the subscripts A and B represent solid species, C for solid intermediate, and D and E for intermediate and final product gases, respectively. The species equations that are solved together with equation (2) for high explosives then become

$$\rho_e \frac{\partial Y_A}{\partial t} = -r_1 \tag{7}$$

$$\rho_e \frac{\partial Y_B}{\partial t} = r_1 - r_2 \tag{8}$$

$$\rho_e \frac{\partial Y_C}{\partial t} = r_2 - r_3 \tag{9}$$

$$\rho_e \frac{\partial Y_D}{\partial t} = r_3 - r_4 \tag{10}$$

$$\rho_e \frac{\partial Y_E}{\partial t} = r_4 \tag{11}$$

$$Y_A + Y_B + Y_C + Y_D + Y_E = 1 \tag{12}$$

where $Y_i = \rho_i / \rho_e$ is the mass fraction of each energetic component.

Laser thermal boundary condition

The laser-heated thermal boundary conditions follow Ref. [12] with consideration of the radiation.

Figure 3 shows the irradiated thermal boundary conditions of steel on the face of irradiation.

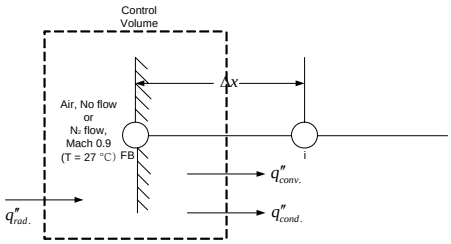

Figure 3. Laser thermal boundary condition of the steel plate - front face.

Two types of heating configurations are used: first, no convective flow at the surface and second, the forced blowing of nitrogen gas at Mach 0.9 for convective flow at the surface. The following balance equation holds at the boundary:

$$q''_{rad.} - q''_{conv.} - q''_{cond.} = 0 \qquad \text{or} \qquad (13)$$

$$\alpha G_{laser} - h(T_{FB} - T_{air}) - k_s \frac{(T_{FB} - T_i)}{\Delta x} = 0 \qquad (14)$$

where $q''_{rad.}$, $q''_{conv.}$ and $q''_{cond.}$ are the heat flux of radiation, convection and conduction. α is temperature dependent absorptivity of steel modeled according to figure 4.

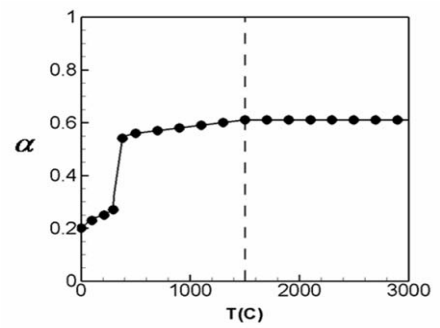

Figure 4. The absorptivity of steel (modeled).

G_{laser} is the intensity of laser given by 200 kW/cm^2 for the experiment being modeled here. h is convection coefficient 500 W/m^2· K for no flow and 2600 W/m^2· K for nitrogen flow at Mach 0.9. T_i is the nodal temperature inside the computational domain at node i, and T_{FB} and T_{air} are the boundary temperature on the surface of steel and the room temperature of air, respectively. The temperature on the front surface T_{FB} is obtained by equating (14).

The thermal boundary condition on the back face of steel plate is shown in figure 5.

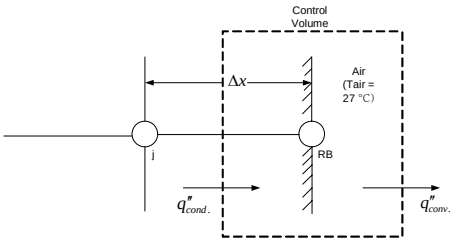

Figure 5. Thermal boundary condition of steel plate – rear face.

Here, the conductive heat flux into steel is positive while the negative convective heat flux leaves the control volume by cooling of the air at ambience. The balance equation for rear surface becomes

$$q''_{cond.} - q''_{conv.} = 0 \qquad \text{or} \qquad (15)$$

$$k_s \frac{(T_j - T_{RB})}{\Delta x} - h(T_{RB} - T_{air}) = 0 \qquad (16)$$

where T_j and T_{RB} are the nodal temperature inside the rear surface at j and temperature on the back face of steel, respectively. Then T_{RB} is obtained by the equation (16). The boundary condition for the RDX heating via HEL behind a steel plate uses the same temperature profile as the rear face of steel without nitrogen flow. In the case of CO2-laser ignition of HMX and TATB, the thermal boundary conditions considered include radiative heat flux. Here the no convection and perfect absorption of radiative heat flux are assumed. The balance equations for HMX and TATB at the wall follow

$$q''_{rad.} - q''_{cond.} = 0 \qquad \text{or} \qquad (17)$$

$$\alpha G_{laser} - k_e \frac{(T_{FB} - T_i)}{\Delta x} = 0 \qquad (18)$$

where α is set to 1 implying a perfect absorption of radiative flux. The temperature of rear face of HMX and TATB can be obtained by solving the equation (18).

Result

In the experiment [7], a steel coupon of 1.5 mm thickness is exposed to five pulses at 100 J/cm^2 per pulse. The experiment is repeated with and without convective nitrogen flow at Mach 0.9. The temperature on the back side of the coupon is measured. Figure 6 shows calculated temperature profiles of steel on the front face at each incidence of laser pulse. Five peaks in the plot correspond to five pulses of laser incidence on the front surface. The mean temperature rise in (b) with convective flow is less than (a) without, as shown in the figures.

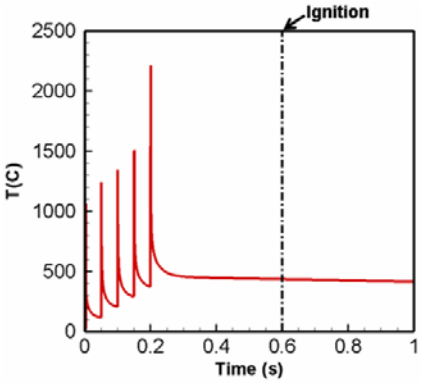

(a)

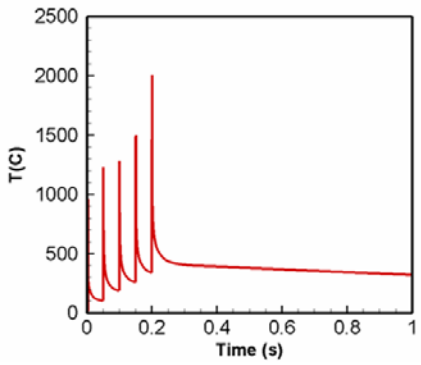

(b)

FIGURE 6. The temperature profiles of steel coupon - front face: (a) no flow (air only), (b) nitrogen flow at Mach=0.9.

The calculation aimed at reproducing the laser heating experiment [7] is shown in figure 7. The rise in temperature on the front side of steel in figure 6 show five multiple peaks leading to an average temperature of 500 C at 0.2 second. The calculated thermal response of steel on its rear side shown in figure 7 explains how the laser energy absorbed is conducted across the metal of 1.5 mm thickness. The linear temperature drop from 450C in both cases with and without the forced cooling is compared with calculation and actual laser experiment. The quantitative comparison of the present calculation to the laser heating data is achieved in this paper.

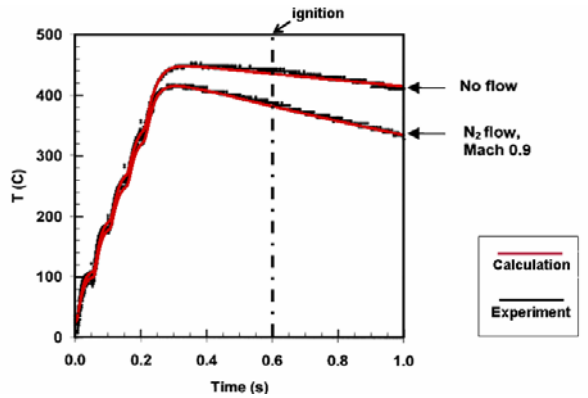

FIGURE 7. The temperature profiles of steel coupon - rear face (Experimental data from [7]).

Next, the same pulsed laser heating is applied to a confined energetic system that consists of RDX contained in a steel casing of 1.5 mm thickness. This is a prototype for laser-heating and igniting test of confined explosive in munitions of general purpose, for instance. The choice of RDX is for its well-characterized chemico-thermal properties developed previously [13]. The same multiple pulses are applied at the exterior of its confinement. The heat transfer process along with irradiative and convective flow conditions heats the inner side of the steel that is in contact with the energetic material. Figure 8(a) depicts the ignition event produced by the present calculation. At approximately 590ms after the start of five laser pulses, the ignition is observed with a sudden increase in temperature, reaching beyond 3300C. The complete formation of final product gas (mass fraction=1.0) further confirms the progress of the multi-step fast deflagration process of RDX. The conceptual setup used in this exercise may represent a prototypical confined energetic system exposed to a high energy laser beam. Well-characterized high explosive such as RDX together with a material model for steel that uses temperature dependent material properties are excellent showcase of current numerical models that can be extended to a series of other laser-kill type applications.

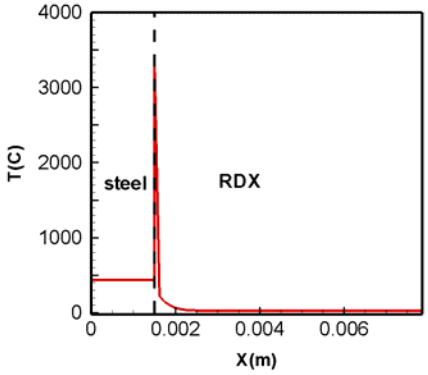

(a)

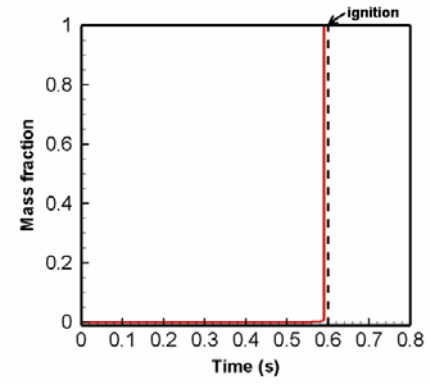

(b)

FIGURE 8. The calculated temperature of steel with RDX and mass fraction at 590.821 ms: (a) Temperature profile; (b) The mass fraction of RDX on the contact face.

Two additional tests are conducted to validate the laser heating work through the laser experimental data obtained from the open (as opposed to a confined) explosive ignition discussed in [6]. In this exercise, we predict the time to ignition for high explosives upon continuous laser irradiation on an explosive pellet of 1.25cm diameter. In addition to RDX, other choices of well-characterized explosives we consider include TATB and HMX [11]. Tables 1 through 4 are the deflagration kinetic parameters fitted earlier to the ODTX measurements. In order to reproduce the laser data in [5, 14], the pre-exponential factor ln *Z* term is modified to accommodate the faster exothermic response of heated non-confined explosive pellets exposed to a direct laser light.

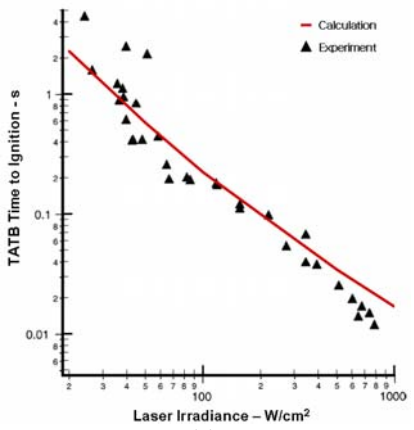

(a)

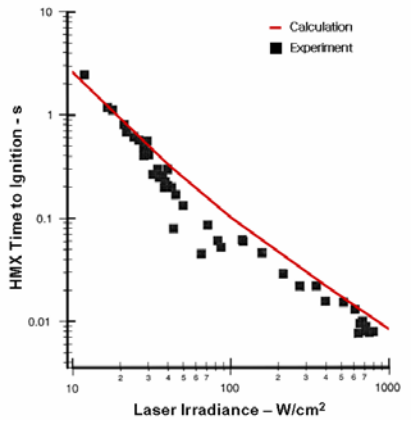

(b)

FIGURE 9. Unconfined HE ignition via direct laser irradiation shown for TATB and HMX: (a) TATB, (b) HMX.

In both cases of laser ignition of TATB and HMX, the calculated time-to-ignition well represents the measurements reported in [5].

Conclusion

We have developed a model of the laser-induced thermal heating and ignition of confined energetic materials. Quantitative comparisons of calculations to experimental measurements are made. The model allows us to predict time-to-explosion of confined energetic materials as found in general weapon system subject to a high energy laser (both pulsed and continuous type) irradiation. Three- and four-step global chemical kinetics previously developed for thermal decomposition of high explosives using electric heater required adjustments in the pre-exponential terms. This adjustment for using faster rate in laser ignition of TATB and HMX is consistent with the previous observation. The present model for laser ignition of confined energetic materials will provide effectiveness guidelines for laser shooting of an energetic system such as the ballistic missiles.

Acknowledgments

This work was supported by Korea Research Foundation Grant funded by the Korea Research Foundation (KRF-2006-311-D00038), the High Energy Materials Research Center (ADD-HM-20, 22) and the Brain Korea 21 project through the Institute of Advanced Aerospace Technology at Seoul National University. Scientific discussion with Dr. A. Gojani is warmly acknowledged.

References

1) A. E. Wynne, B. C. Stuart, “Rate dependence of short-pulse laser ablation of metals in air and vacuum,” *Applied physics A* 76, 373-378 (2002).
2) J. Mazumder, W. M. Steen, “Heat transfer model for cw laser material processing,” *Journal of Applied Physics* 51, 941-947 (1980).
3) J. K. Chen, J. E. Beraun, L. E. Grimes, “Short-time thermal effects in thermomechanical response caused by pulsed lasers”, *Journal of Thermophysics and Heat Transfer* 17, 35-42 (2003).
4) B. N. Chichkov, C. Momma, S. Nolte, F. von Alvensleben, A. Tunnermann, “Femtosecond, picosecond and nanosecond laser ablation of solids,” *Applied Physics A*, 63, 109-115 (1996).
5) A. N. Ali, S. F. Son, B. W. Asay, M. E. Decroix, “High-irradiance laser ignition of explosives,” *Combustion Science and Technology* 175, 1551-1571 (2003).
6) C. M. Tarver, “Chemical kinetic modeling of HMX and TATB laser ignition tests,” *Journal of Energetic Materials* 22, 93-107 (2004).
7) C. D. Boley, A. M. Rubenchik, “Modeling of high-energy pulsed laser interactions with coupons,” LLNL Technical Report, 2003, UCRL-ID-151857.
8) J. J. Yoh, M. A. McClelland, J. L. Maienschein, A. L. Nichols, and C. M. Tarver, “Simulating thermal explosion of octahydrotetranitrotetrazine-based explosives: model comparison with experiment,” *Journal of Applied Physics* 100, 073515(2006).
9) R. Hultgren, P.D. Desai, D. T. Hawkins, M. Gleiser, K. K. Kelley, Selected values of the thermodynamic properties of the elements, American Society of Metals, p. 185 (1973)..

10) Y. S. Touloukian, "Thermophysical properties of matter," Vol. 1, Thermal conductivity, Metallic Elements and Alloys, IFI/Plenum, NY, p. 169 (1970).
11) J. J. Yoh, K. H. Kim, "Shock compression of condensed matter using Eulerian multi-material method: Applications," *Journal of Applied Physics*, submitted (2007).
12) S. V. Patankar, Numerical heat transfer and fluid flow, Taylor & Francis, (1980).
13) J. J. Yoh, M. A. McClelland, J. L. Maienschein, J. F. Wardell, and C. M. Tarver, "Simulating thermal explosion of octahydrotetranitrotetrazine-based explosives: model comparison with experiment," *Journal of Applied Physics* 97, 083504 (2005).
14) K. C. Lee, K. H. Kim, J. J. Yoh, "Modeling of high energy laser ignition of energetic materials," *Journal of Applied Physics*, submitted (2007).

TABLE (1). Thermal and chemical parameters for TATB.

	TATB	Solid intermediate A	Solid intermediate B	Gaseous products
1. Initial density (g/cm^3)	1.835			
2. Heat capacity (cal/g-K) at 573 K	0.45	0.39	0.29	0.29
3. Thermal conductivity (cal/cm-g-K) at 573 K	1.10×10^{-3}	5.50×10^{-4}	2.70×10^{-4}	1.00×10^{-4}

TABLE (2). Reaction rate parameters for TATB.

Reaction step	$\ln Z$	E(kcal/mol)	Reaction order	Heat of reaction q(cal/g)
1	48.0	60.0	1	+50.0
2	35.8	42.0	1	+50.0
3	36.8	33.8	2	-700

TABLE (3). Thermal and chemical parameters for HMX.

	Solid-β	Solid-δ	Solid intermediate	Gases intermediate	Gaseous products
1. Initial density (kg/m^3)	1865				
2. Heat capacity (J/kg°C)	1190	1190	1190	1422	1422
3. Thermal conductivity (W/m°C)	0.456	0.456	0.456	0.1034	0.1034

	Viton	
	Solids	Gases
1. Initial density (kg/m^3)	1830	1830
2. Heat capacity (J/kg°C)	1005	1131
3. Thermal conductivity (W/m°C)	0.26	0.4188
4. $\ln Z$	32.70	

TABLE (4). Reaction rate parameters for HMX.

Reaction step	$\ln Z$	E(kcal/mol)	Reaction order	Heat of reaction q(cal/g)
1	49.13	48.47	1	+10.0
2	56.7	52.70	1	+60.0
3	52.8	44.30	1	-133.0
4	50.1	34.10	2	-1337.0